Neuroinform (2013) 11:91–103
DOI 10.1007/s12021-012-9159-9

ORIGINAL ARTICLE

System for Integrated Neuroimaging Analysis and Processing of Structure

Bennett A. Landman · John A. Bogovic · Aaron Carass · Min Chen · Snehashis Roy · Navid Shiee · Zhen Yang · Bhaskar Kishore · Dzung Pham · Pierre-Louis Bazin · Susan M. Resnick · Jerry L. Prince

Published online: 30 August 2012

Abstract Mapping brain structure in relation to neurological development, function, plasticity, and disease is widely considered to be one of the most essential challenges for opening new lines of neuro-scientific inquiry. Recent developments with MRI analysis of structural connectivity, anatomical brain segmentation, cortical surface parcellation, and functional imaging have yielded fantastic advances in our ability to probe the neurological structure-function relationship *in vivo*. To date, the image analysis efforts in each of these areas have typically focused on a single modality. Here, we extend the cortical reconstruction using implicit surface evolution (CRUISE) methodology to perform efficient, consistent, and topologically correct analyses in a natively multi-parametric manner. This effort combines and extends state-of-the-art techniques to simultaneously consider and analyze structural and diffusion information alongside quantitative and functional imaging data. Robust and consistent estimates of the cortical surface extraction, cortical labeling, diffusion-inferred contrasts, diffusion tractography, and subcortical parcellation are demonstrated in a scan-rescan paradigm. Accompanying this demonstration, we present a fully automated software system complete with validation data.

Keywords Brain · MRI · Cortical surface · White matter parcellation · Fiber tracking · Sub-cortical segmentation

Introduction

Understanding the relationship between structure and function in the brain is a crucial goal in neuroscience, and the role of imaging technology has been an important part of this research process for well over 20 years (Pechura & Martin 1991). Over this time period, image acquisition capability has expanded tremendously from the core

B. A. Landman (✉)
Department of Electrical Engineering, Vanderbilt University,
2301 Vanderbilt Pl., Station B, PO Box 351679, Nashville, TN
37235-1679, USA
e-mail: bennett.landman@vanderbilt.edu

B. A. Landman · J. L. Prince
Department of Biomedical Engineering,
Johns Hopkins University,
Baltimore, MD, USA

B. A. Landman
The Department of Radiology and Radiological Sciences,
Vanderbilt University,
Nashville, TN, USA

J. A. Bogovic · A. Carass · M. Chen · S. Roy · N. Shiee ·
Z. Yang · D. Pham · J. L. Prince
Department of Electrical and Computer Engineering, Johns
Hopkins University,
Baltimore, MD, USA

B. Kishore · D. Pham · J. L. Prince
The Russell H. Morgan Department of Radiology and
Radiological Sciences, Johns Hopkins University School
of Medicine,
Baltimore, MD, USA

D. Pham
Center for Neuroscience and Regenerative Medicine,
Washington, DC, USA

S. M. Resnick
Laboratory of Personality and Cognition, National Institute on
Aging,
Baltimore, MD, USA

P.-L. Bazin
Department of Neurophysics, Max Plank Institute for Human
Cognitive and Brain Sciences,
Leipzig, Germany

technologies of structural MRI and functional PET imaging (blood flow and metabolism) to now include functional MRI (fMRI) and diffusion weighted MRI (DW-MRI). Image processing algorithms originally struggled to segment tissue types and align functional and structural images, but are now routinely delineating and labeling structural MRI data, deformably registering populations of individuals to atlases, and computing patterns of anatomical connectivity throughout the brain. These techniques have in turn enabled population studies using sophisticated statistical analyses from voxel based morphometry (Ashburner & Friston 2000) to small world network analyses (Sporns et al. 2004). Because of these advances, we stand at a new threshold, one that looks for new discoveries in ever increasing imaging data sources and ever increasing numbers of subjects and/or patients under study (e.g., (Thambisetty et al. 2010), (Mueller et al. 2005)). Beginning now and continuing into the future, neuroscientists will require more routine analysis of increasingly larger populations with algorithms that have certified, reliable capabilities and limited need for human involvement for manual verification.

Numerous packages for quantitative brain image analysis are publicly available, including BrainSuite (Shattuck & Leahy 2000), BrainVisa (Cointepas et al. 2001), BrainVoyager (Brain Innovation 2007), Caret (Van Essen et al. 2001), FSL (Smith et al. 2004), FreeSurfer (Fischl et al. 1999; Dale et al. 1999), the NA-MIC kit (Pieper et al. 2006), and SPM (Friston 2006). Each of these packages offers different capabilities and tools for performing various types of analyses such as segmentation, registration, functional image analysis, and diffusion-weighted image analysis. An advantage of the availability of such diverse image analysis packages is that capabilities from competing packages are frequently complementary. Each of these packages may possess algorithms that are more ideally suited for different applications, and each has a user interface that may appeal to different users. Increasing the landscape of neuroimaging analysis packages benefits not only neuroscientific users of the software, but also developers who gain additional resources for benchmarking new algorithms. The emergence of common, research-oriented file formats (e.g., NIfTI) has enabled the interoperability of these major packages and custom designed tools. JIST encapsulates MIPAV's extensive image file format libraries for and supports over 70 common and proprietary data structures. For complete details, please see the MIPAV documentation (http://mipav.cit.nih.gov/pubwiki/index.php/Supported_Formats).

This paper describes a new pipeline for the multimodal analysis of neuroimaging data, the System for Integrated Neuroimaging Analysis and Processing of Structure (SINAPS). The elements of this pipeline have been reported elsewhere in work of both our own group and others—e.g., (Bazin & Pham 2007a; Han et al. 2004; Mori et al. 1999). Here, we describe incorporation of improvements to these algorithms as well as a previously unpublished dura removal stage aimed at making the elements of the analysis work well together in a fully automated manner. The SINAPS suite of computational tools (illustrated in Figs. 1 and 2) includes the (1) automatic extraction of brain tissue and exclusion of non-brain tissue, (2) segmentation of cortical, subcortical, and white matter lesion tissues, (3) cortical surface reconstruction, (4) gyral labeling, and (5) white matter tract segmentation.

SINAPS features several desirable properties for neuroscientific applications. First, the algorithms are designed to take advantage of multiple MR contrasts. For example, the use of both a structural T1-weighted contrast and a FLAIR contrast, which provides lesion enhancement, can be used in combination to obtain whole brain segmentations that include delineation of white matter lesions. Second, topology preservation is obtained not only for the cerebral cortex, but for most major brain structures. This allows the results of the algorithms to be readily utilized for group shape analyses that employ high-dimensional diffeomorphic transformations (Beg et al. 2005). Third, a full DW-MRI pipeline is married to this foundation by careful independent processing of the DW-MRI (including motion correction of the separate gradient images) followed by deformable registration of these data to the structural data in order to remove geometric distortion caused by EPI acquisitions and magnetic susceptibility. Deterministic tractography is carried out and a novel white matter tract labeling method provides labels of the spatial volumes that are occupied by the major white matter tracts (Bazin et al. 2011). In order to accommodate and measure white matter lesions commonly found in older subjects, lesions are automatically segmented and quantified for determining lesion load measures. Fourth, the algorithms have been designed to be reasonably efficient, enabling results to be obtained on the order of hours rather than days. The cortical reconstruction algorithm, in particular, employs a level set deformable surface model that is known to possess computational advantages over parametric deformable models (Han et al. 2004). Therefore, SINAPS is ideally suited for the simultaneous study of anatomical structure including white matter lesions together with diffusion MRI including conventional diffusion contrasts as well as tractography.

The core algorithms have been validated individually elsewhere using comparison to manual raters, repeatability experiments, and simulations. Therefore, the accuracy against a gold standard in each of the elements of the algorithm have been (in most cases) previously determined. The new pipeline reported here is validated in a repeatability experiment involving 21 subjects scanned twice each at 3T (Landman et al. 2011). The objective of this study is aimed therefore at demonstrating new analytic capabilities that

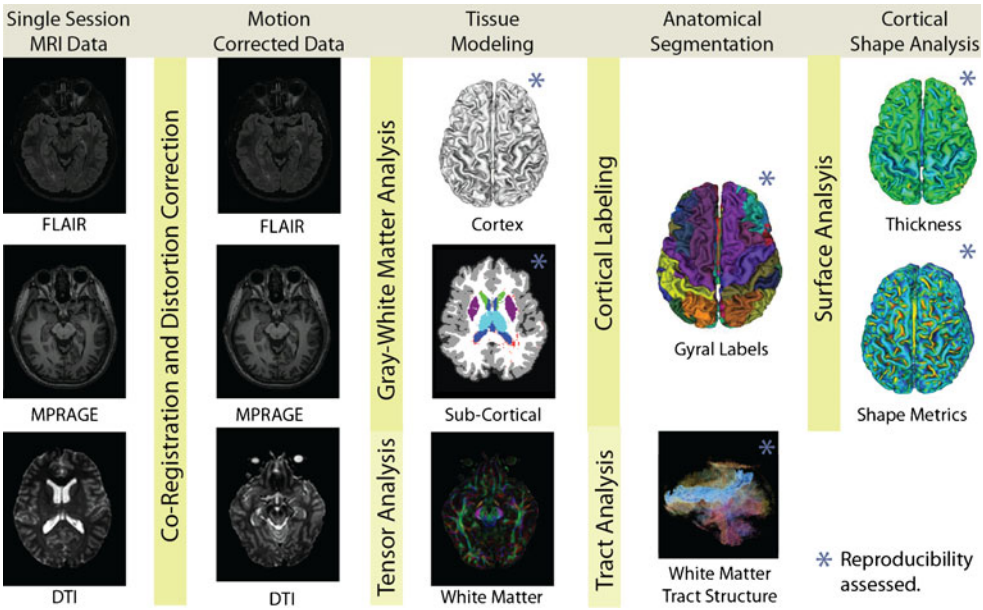

Fig. 1 Illustration of processing steps in SINAPS. First, all data within each session (including FLAIR to highlight lesions, MPRAGE for structural detail, and DTI for WM structure) are co-registered. Then, the cortical and sub-cortical anatomies are inferred from the structural scans while local orientation properties are inferred from the DTI data. The cortical surface is labeled into anatomical divisions while the DTI data are segmented into tract structures. Finally, the cortex characteristics are summarized with thickness and shape metrics

become possible with integrated multimodal analysis and to provide the necessary statistical data for determination of effect size requirements in new neuroscience studies that would look to study structural and connectivity differences or changes in a population.

Methods

The follow sections detail the modules which compose the SINAPS pipeline. The data dependencies between the modules are explained in Table 1. Modules have been evaluated in the form captured by Toads-CRUISE Release R3c (March 23, 2012) with MIPAV 5.4.1. Details of all non-default parameters are included below. All tools have been released freely as open-source software. These tools support standard file formats and data structures, permitting interoperability with other available packages using the Java Image Science Toolkit (JIST) (Lucas et al. 2010) and the Medical Image Processing and Visualization (MIPAV) software. JIST provides the ability to visualize algorithms and procedures through high level block-diagrams along with classical dialog box and command line user interfaces (Covington et al. 2010, 2011).

***JIST Details*:** *The combined tissue segmentation and cortical surface estimation pipeline is wrapped in a single*

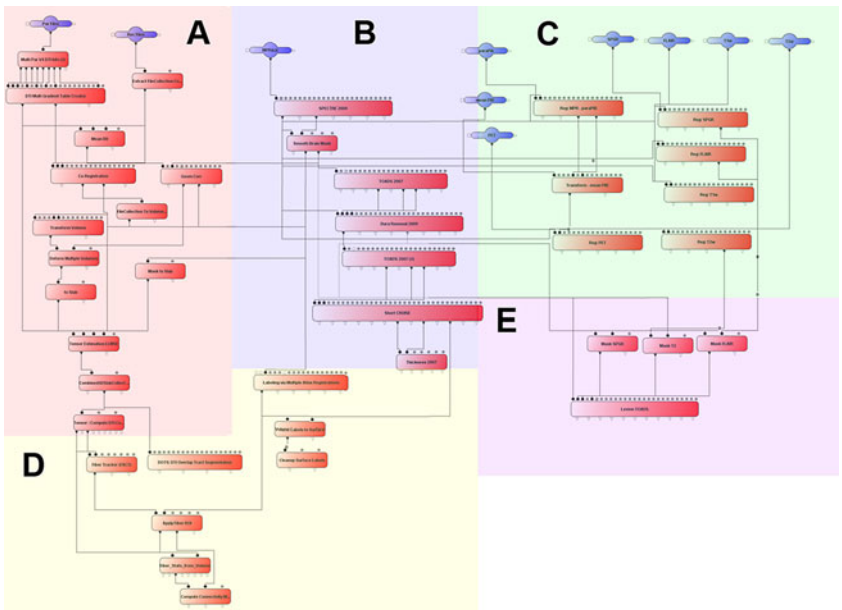

Fig. 2 Screen shot of JIST Layout with color overlaying indicating functionality of sub-layouts: **a** CATNAP, **b** CRUISE, **c** co-registration, **d** gyral-labeling and segmentation, and (E) lesion segmentation

Table 1 Data-dependency structure for SINAPS modules

Stage	Method	Module	MPRAGE	FLAIR	DTI	Brain mask	Cortical structure	Tensors	Fiber tracts	WM labels
Data acquisition			C	C	C					
Pre-processing										
	Brian isolation	SPECTRE	U			C				
	Brain segmentation	Lesion-TOADS	U	U		U	C			
Cortical surface estimation										
	Dura removal	Remove dura				M	U			
	Sulci enhancement	ACE					U/M			
	Surface identification	CRUISE					U/M			
	Surface labeling	Multi-atlas	U	U			U/M			
White matter labeling										
	Tensor estimation	CATNAP			U			C		
	Tractography	Fiber tracker						U	C	
	Tract segmentation	DOTS						U		C

For each data processing step (rows): **C** indicates that a dataset is created, **U** indicates that the dataset was used, and **M** indicates that the dataset is modified

module: "TOADS-CRUISE (1.7T)" Module. In this work, each component was run separately.

Brain Extraction

Brain extraction (a.k.a., skull stripping or brain isolation), is equivalent to a whole brain segmentation which separates gray matter (GM) and white matter (WM) from other tissues such as cerebrospinal fluid (CSF), skull, meninges, etc. The primary difficulty in this task is the lack of discernible contrast between many of the tissues types that compose the extra-cerebral tissue and the brain. SINAPS uses the Simple Paradigm for Extra-Cerebral Tissue Removal (SPECTRE) (Carass et al. 2011) module to extract brain from non-brain tissue by combining elastic registration with atlas-based priors, tissue segmentation, and morphological techniques (guided by a watershed principle). SPECTRE was specifically designed to include a thin layer of CSF surrounding the cortical surface thus avoiding unnecessary removal of any cortical gray matter, which would adversely affect cortical reconstruction.

***JIST Details*:** "SPECTRE 2012 (1.3R)" Module.

Brain Segmentation

The anatomy of the human brain has a rich structure, with extremely convoluted and complex shapes like the cerebral cortex or the ventricles. However, the topological properties of the segmented brain structures are very simple, dictated by the normal neurological developmental process. Neuroimaging research has focused on topology for the study of the cerebral cortex; with a few simplifying assumptions, one can model the cortex topologically as a hollow sphere. With this model, the highly convoluted surface of the brain can be flattened into a plane, a sphere, or a partially flattened surface and structural or functional information can be visualized and analyzed more easily (Tosun et al. 2003; Thompson & Toga 2002).

We extended topological constraints to describe multiple object relationships in the segmentation of brain structures using the TOpology-preserving Atlas Driven Segmentation (TOADS) (Bazin & Pham 2007a). The TOADS topological model extends the early work of (Mangin et al. 1995) to maintain relationships between all the structures to be segmented, while integrating features from tissue segmentation methods (Pham & Prince 1999; van Leemput et al. 1999). Topological constraints prevent holes from occurring in a particular structure and therefore suppress anomalies stemming from noise, making the method robust even without spatial regularization. Because the topology is preserved during the segmentation, no topology correction is required when extracting the cortex. Segmented structures include cerebral the cortical gray matter, cerebral white matter, cerebellar gray matter, cerebellar white matter, brainstem, ventricles, caudate, putamen, thalamus, and sulcal cerebrospinal fluid. Details on the algorithm are given in (Bazin & Pham 2008).

***JIST Details*:** "TOADS 2009 (1.6R)" Module. *Parameter notes: Output image: cruise inputs.* This module was not used. Rather, we used the robust variant described below.

Lesions in a Topology-Preserving Framework

Characterizing neuroimaging abnormalities plays an important role in investigating both normal development/aging

and disease processes. In particular, white matter lesions are frequent findings which can be troublesome for automated analysis methods. Lesions do not have a fixed topology, so they cannot be directly incorporated into a TOADS topological atlas. However, since white matter lesions occur within white matter, we can model them in a topological framework by considering the union of lesion and normal tissue as one object. From a topological point of view, normal appearing structure and lesions together represent the structure as it would appear in a normal brain. Intensity based classification is used to identify lesions within the white matter.

In a multi-channel framework, each MR input image provides plausible contrast for only a subset of the desired structures. These contrasts on different MR pulse sequences can cause inaccuracy in the segmentation of both lesions and brain structures, revealing the need for a more effective use of the intensity information from each of the input channels (Shiee et al. 2008). Although T2-weighted and FLAIR images have the best contrast for lesions, the intensity distribution of lesions has considerable overlaps with those of healthy tissues in these types of MR images, making the intensity based lesion segmentation techniques vulnerable to false positives. These types of misclassifications are prominent especially at the boundaries of WM with other structures (GM and ventricles). Thus, they can be suppressed by penalizing the lesion membership in the vicinity of the WM boundaries. We use a boundary distance function re-weighting factor to remove the false positives without hindering the detection rate of lesions close to the WM boundaries (see (Shiee et al. 2010)).

***JIST Details*:** "Lesion TOADS (1.5R)" Module.

Cortical Surface Estimation

Once the brain tissue has been classified into topologically correct tissue objects, locating the cortical manifold, including the pial surface, central surface, and inner gray matter surface is, *in theory*, a simple matter of finding the corresponding surfaces of the cortical gray matter object. In practice, however, additional processing steps lead to substantially improved accuracy and robustness. The brain extraction method, SPECTRE, is designed to be conservative in the amount of tissue removed as to prevent algorithmically induced brain loss. A second-pass dura removal step, described below, is used to refine the brain extraction and reduce contamination of dura signal in the cortical manifold. Subsequently, the brain segmentation techniques produce tissue classifications topologically consistent at the voxel-wise level, typically at millimeter resolution. Memory and time constraints make imaging and direct analysis at higher resolution impractical. However, using a feature enhancement technique and a topologically consistent deformable model, we can capture sub-voxel characteristics of the cortical manifold.

***JIST Details*:** *The combined cortical surface estimation pipeline is wrapped and was evaluated as a single module:* "CRUISE (1.2T)" Module. Each component is also available to run separately.

Dura Removal

Brain extraction with SPECTRE occasionally fails by leaving wedges of dura with similar contrast to that of gray matter. To remove these artifacts, we developed a second-pass dura removal procedure which runs after an initial tissue segmentation. The union of the GM and WM memberships is topologically correct. Using the inner component of this union (i.e., the WM membership) as the initialization, we then run a topology-preserving geometric deformable (TGDM) surface model (Han et al. 2003) between the topologically corrected WM membership and the union of the GM and WM memberships. Here we include an additional force to regularize the thickness between the two memberships. The regularizing force effectively prunes segments of dura that might be attached to the gray matter via irregular or thin connections using fast marching topology correction of membership (Bazin & Pham 2007b). The resultant pial surface level set is used to generate a final brain extraction mask, which is then applied to the original image.

***JIST Details*:** "Remove Dura 2009 (1.6 RC)" Module.

Sulci Enhancement

Partial volume effects limit the achievable resolution at which the cortical manifold may be studied due to apparent inconsistencies in surface morphology/topology when data are viewed at voxel resolution. The problem is most acute in sulcal regions where the cortical gyri are "back-to-back" with a subvoxel gap between neighboring tissue groups. Other groups have used cortical thickness constraints to produce reasonable results in these regions, cf. (MacDonald et al. 2000; Zeng et al. 1999). We use the anatomically consistent enhancement (ACE) procedure to modify the initial GM segmentation to create a thin, digital separation between sulcal GM banks (Xu et al. 1999; Han et al. 2001). This is done so as to separate sulcal GM from opposing banks allowing for the generation of accurate central and outer surfaces. ACE automatically locates the exterior skeleton of the GM/WM interface and reduces the GM membership value on the skeleton, thus changing this local GM values into CSF. Use of a conventional Euclidean skeleton will "gouge" the GM indiscriminately, regardless of the presence of actual CSF. ACE incorporates the presence of CSF in the definition of the distance used to compute the

outer skeleton, where a weighted distance measure leads to a more appropriate division. A similar approach was also described in (Riviere et al. 2002). In sulci where there is no evidence of CSF, the distance will default back to the Euclidean definition, and the gyral banks will be split equally—a reasonable assumption given a lack of external information.

***JIST Details*:** "Gray Matter Enhance (1.3 RC)" Module.

Surface Identification

The previous steps have set the stage for the estimation of the three cortical surfaces (i.e., outer pial surface, central surface, and inner GM/WM surface) using a deformable surface model method, which we refer to as nested cortical reconstruction using implicit surface evolution (CRUISE). The heart of the deformable method is a topology-preserving geometric deformable (TGDM) surface model (Han et al. 2003). TGDM distinguishes itself from parametric deformable models and standard geometric deformable models (GDMs) in that it preserves the topology of the evolving shape using a subtle but important modification to the standard level set implementation (Sethian 1999). The resulting narrow band algorithm remains computationally efficient, requiring only a 7 % time penalty in order to maintain object topology during evolution.

The surface estimation follows the original CRUISE presentation (Han et al. 2004). The inner cortical surface is initialized with the topologically correct binary WM segmentation. An outward curvature force drives the boundary surface to the 0.5 isosurface of the continuous WM membership density function while maintaining topological consistency. The outer cortical surface is found by driving toward the 0.5 isosurface of the sum of the continuous WM and GM membership functions. Finally, the central surface is found as the topologically consistent surface within the GM membership and sitting between the WM and CSF membership functions.

***JIST Details*:** "Nested TGDM (1.3 R)" Module.

Surface Labeling

Cortical labels corresponding to traditional neurological definitions are estimated through multi-atlas registration, label fusion, and topological correction. First, a collection of atlases derived from the OASIS dataset (Marcus et al. 2007) are non-rigidly registered to a subject's structural image. Labels are transferred from cortical atlases through deformation of the label fields. Differences between the atlas labels in subject space are reconciled using statistical fusion techniques.

Five brains from the OASIS dataset with labels from the Desikan protocol (32 labels per hemisphere) were used as atlases. The atlas registrations are performed via a multi-channel deformable registration technique (Chen et al. 2010) based on the adaptive bases algorithm (Rohde et al. 2003). This technique takes an intensity based approach using normalized mutual information as the similarity metric, which has shown to be advantageous in registrations across different modality (Maes et al. 1997; Viola & Wells 1995). The algorithm constructs a deformation map as an accumulation of radial basis functions under a hierarchical schema. By using compact support RBFs, non-overlapping regions in the image can be optimized locally, hence reducing both computational complexity and run time. We account for the multiple image channels as weighted contributions within the deformable registration framework through a vectorized calculation of the difference metric. Incorporating information from multiple channels allows the final deformation to represent anatomically variability that may only be discernible in certain image contrasts, thus making the most of all available image channels.

To fuse the atlas labels together on the cortical surface of the subject we have developed an extension (Bogovic et al. 2010) to the STAPLE algorithm (Warfield et al. 2004). STAPLE simultaneously estimates a true segmentation and a reliability characterization for each atlas in a collection and was originally presented on voxel level data that included a Markov random field to model spatially correlated structures. Our extended approach operates on surface labels with a mesh-based Markov random field to account for spatial consistency of multiple labels on a mesh. After estimation, a secondary topological correction step is performed in which holes in the label definitions are filled.

***JIST Details*:** "Surface Labeling via Multiple Atlases (1.5 alpha)" Module.

Surface Assessment

We use level set subtraction to estimate cortical thickness as described in (Han et al. 2001). In this approach, cortical thickness is computed from the image volume using distance transforms from the inner to the outer surface. A thickness value is assigned to each voxel in the volume between the two surfaces and is defined as the sum of the distances from the voxel to each of the two surfaces. The reconstructed cortical surface is generated in the same coordinate space as the image volume, which means that each vertex of a surface mesh can obtain image values by directly mapping into the image data in the volume. Accordingly, we obtain measures of cortical thickness at each surface vertex using trilinear interpolation applied in the image volume containing estimates of cortical thickness at volumetric grid points.

***JIST Details*:** "Thickness (1.3R)" Module.

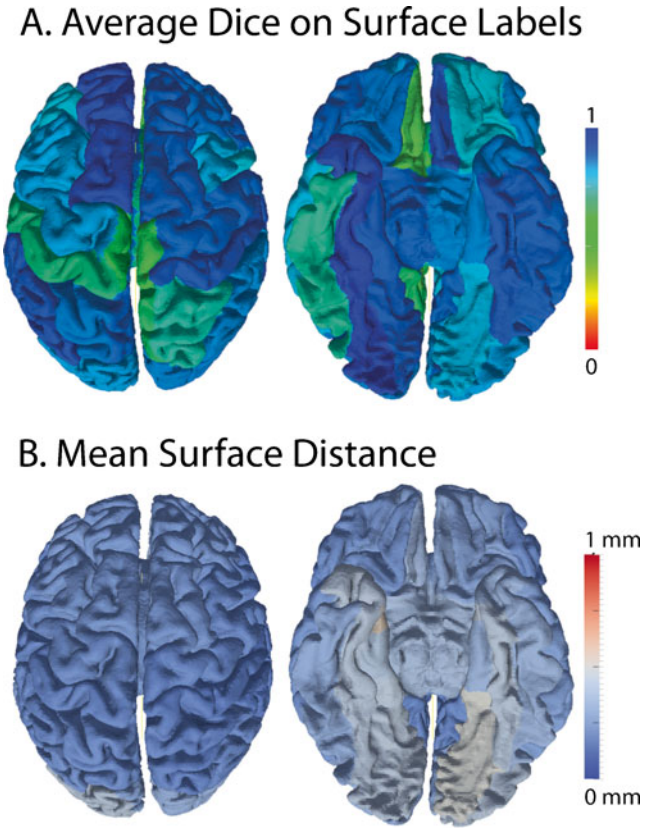

Fig. 3 Reproducibility of cortical surfaces. Average overlap of gyral regions defined on independent scan-rescan dataset was greater than 0.8 Dice (**a**), while the mean surface distance between the scan-rescan cortical surfaces was less than a millimeter (**b**)

White Matter Tract Labeling

In the SINAPS pipeline, we integrate DTI and structural processing by assimilating CATNAP (Landman et al. 2007). To process the DW-MRI data, images are co-registered to account for motion and distortion, the gradient tables are corrected for the anatomical position relative to diffusion sensitization, and diffusion tensor sand tensor contrasts are computed. A significant challenge in the use of DTI measures in conjunction with anatomical T1 and T2 scans is the presence of eddy-current and susceptibility induced distortions in diffusion weighed images acquired with echo planar imaging (EPI). A number of strategies have been shown to be useful in correcting for these distortions: registration (Rohde et al. 2004), reverse-gradient (Andersson et al. 2003), and field-mapping methods (Jezzard & Balaban 1995; Jezzard et al. 1998). With SINAPS, we use the mutual-information registration approach since, unlike reverse-gradient or field mapping techniques, registration methods do not require additional MR image acquisitions (which are typically highly idiosyncratic to a scanner or institution). Specifically, the undistorted anatomical MR modalities (usually MPRAGE) are used as registration targets to correct the geometry of the distorted EPI diffusion weighted acquisitions. This scheme simultaneously corrects geometric distortion and co-registers the diffusion-weighted images to structural images, tightly coupling the two and facilitating the computation of measures derived from both modalities. Note that the distortion correction is currently not constrained to be in the phase-encode direction.

***JIST Details*:** 'CATNAP (1.3 beta)' Module. Note that the individual processing steps that make up the CATNAP module are also available separately.

Tractography

The rise of DW-MRI has been, in large part, attributed to the ability to infer the presence of large-scale oriented tracts within apparently (on traditional MRI) homogeneous white matter (Mori et al. 1999). A recent review of diffusion imaging and tractography is given by Derek Jones (Jones 2008). Herein, we illustrate use of the SINAPS platform to combine diffusion and structural information. In this illustration, we use the cortical labels as targets for the underlying fiber tracts.

JIST Details: 'Fiber Tracker (FACT) (1.4 RC)' Module.

White Matter Tract Segmentation

While fiber tracking provides information about the connectivity between remote regions of the brain, the segmentation of fiber bundles or tracts that correspond to known anatomical atlases requires additional grouping, trimming, and labeling (Maddah et al. 2007; El Kouby et al. 2005; Lawes et al. 2008; Mori et al. 2005). There are a few alternative methods based on level sets (Lenglet et al. 2006), non-parametric fuzzy classification methods (Awate & Gee 2007) for the segmentation of a given bundle from a set of initial regions of interest (ROIs) or using atlases in voxel-based classification techniques (Maddah et al. 2008) and in parametric deformable models (Eckstein et al. 2009). These methods often consider a single fiber bundle or region at a time, without explicitly addressing the fiber crossing problem. We developed a tract segmentation method to classify white matter voxels according to the name of the tract or tracts passing through them following a Markov Random Field (MRF) modeling approach. The algorithm, referred to as Diffusion Oriented Tract Segmentation (DOTS) (Bazin et al. 2011), defines a Markov field directly on the diffusion tensors to separate the main fiber tracts at the voxel level. A given voxel may represent multiple tracts, thereby characterizing tracts crossing within a voxel. A prior model of shape and direction guides the segmentation, and the brain gets fully segmented into 1) known fiber tracts, 2)

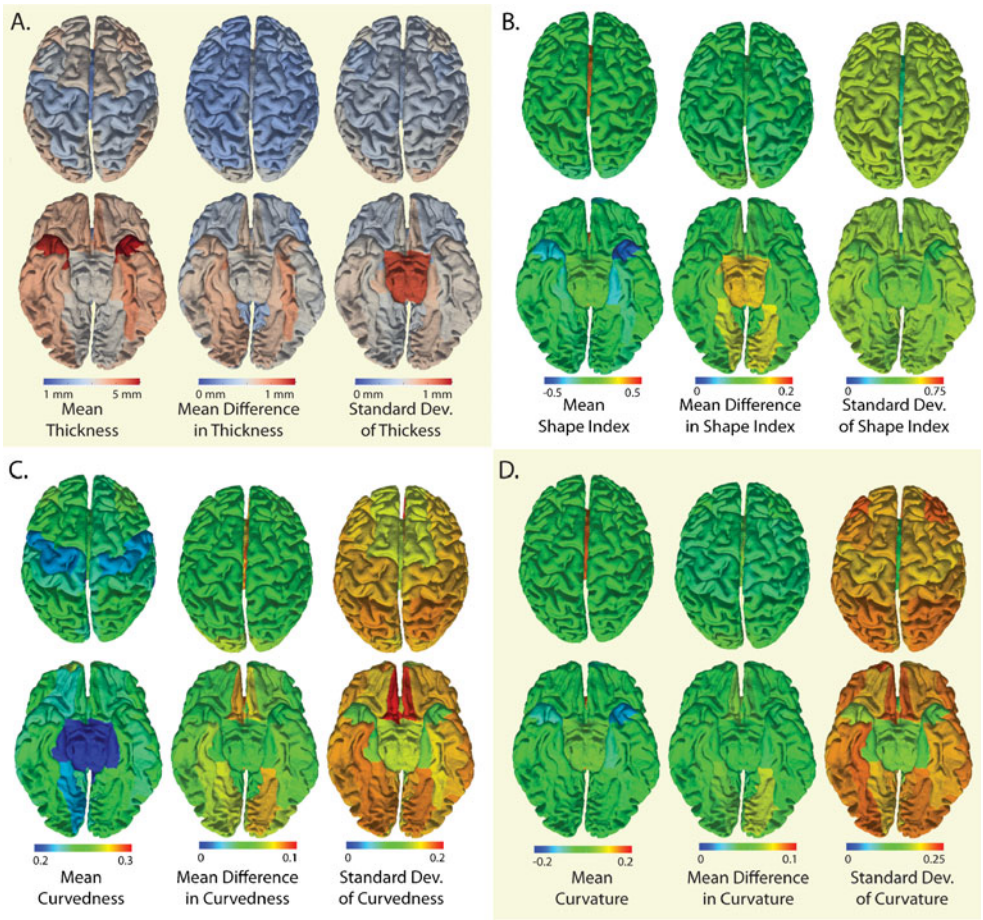

Fig. 4 Mean and variability of surface metrics by gyral region. Mean cortical thickness ranged (**a**) from 1.9 to 4.9 mm with a maximum mean absolute difference of 0.74 mm and an intra-region standard deviation of 0.97 mm. Shape index (**b**), curvedness (**c**), and mean curvature (**d**) showed similar patterns where mean absolute difference was much less than the intra-region variability (on average 20.7 %, 36.7 %, 40.3 %, 24.3 %, respectively)

additional, unspecified fibers, and 3) regions of isotropic diffusion. An atlas describing the probability of tracts throughout the WM voxels was constructed using the underlying data of the Mori and Wakana digital atlas (Mori et al. 2005; Wakana et al. 2007) augmented to include up to 39 different tract labels.

JIST Details: 'DOTS' Module.

Inter-Subject Reproducibility Analysis

To compare findings across subjects, inter-subject registration on partially inflated brains was used. The inflated surfaces are acquired by smoothing the surface with a relaxation operator (described in (Tosun et al. 2004)). The amount of inflation is controlled by a stopping criterion based on the L2 norm of mean curvature (herein, set to 2). MPRAGE images of the repeated scans were registered by affine registration (the 'Optimized Image Registration 3D' Module). Transforms were applied to the FLAIR images with the 'Transform Volume' Module). Average distance between the original surfaces was computed to evaluate the difference between the cortical surfaces generated by two repeated scans.

Results

Scan-rescan multi-modal MRI sessions on 21 healthy volunteers (no history of neurological disease, 11 M/10 F, 22–61 years old) were acquired from the Multi-Modal MRI Reproducibility Resource (Landman et al. 2011). Imaging modalities included whole head acquisitions using MPRAGE (1x1x1.2 mm), FLAIR (1.1×1.1×1.1 mm), and DTI (2.2×2.2×2.2 mm). Scan acquisitions details are provided in the reference. SINAPS was run using the three MRI modalities to extract cortical, sub-cortical, and white matter structure (Fig. 1) independently for 42 scan sessions.

Cortical Surface Reproducibility

The cortical surfaces are one of the essential end-stage products of the SINAPS pipeline (Figs. 1 and 2) and are the results of multi-stage processing (Sections Brain Extraction to Surface Assessment). The average scan-rescan Dice similarity measure between CRUISE surface labels was 0.81 (Fig. 3a). To remove the confounding effects of labeling variability, the following point-wise surface statistics are reported within atlas defined regions. For atlas labeling, the

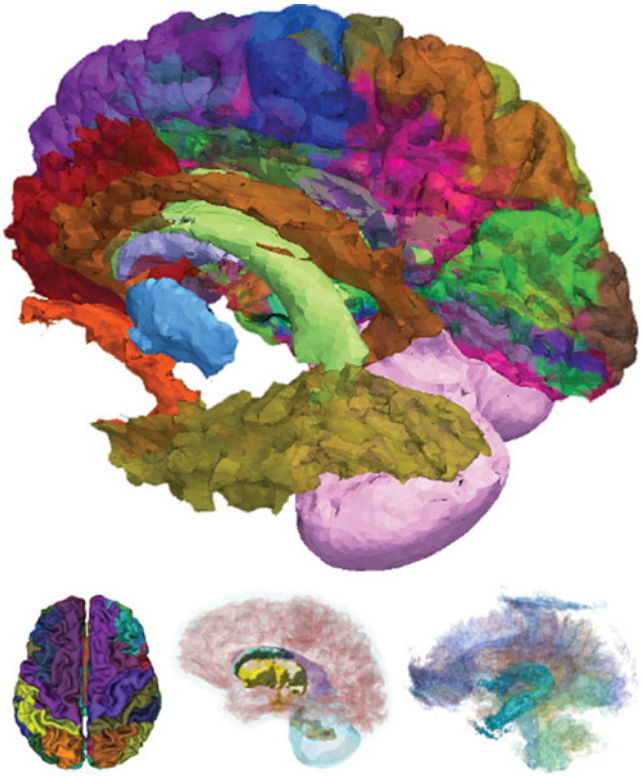

Fig. 5 Illustration of spatial fusion information (*top*) from surface classification (*left*), sub-cortical volumetry (*center*), and white matter tract (*right*) analyses

surfaces were partially inflated and registered. After inter-scan registration, the average distance within a region between the estimated cortical surfaces after rigid body registration was 0.29±0.28 mm. The least reproducible regions were the entorhinal cortex and lingual gyri (0.41–0.54 mm) while 44 of 70 regions exhibited less than 0.29 mm surface differences (Fig. 3b).

Reproducibility of cortical surface properties over all subjects are reported in Fig. 4 by the mean over gyral label, mean absolute difference point-wise, and the standard deviation of the point-wise difference for (**A**) cortical thickness, (**B**) shape index, (**C**) curvedness, and (**D**) mean curvature. These metrics are discussed in (Koenderink & van Doorn 1992). The average cortical thickness was 3.26±0.97 mm (shown in Fig. 4a). For all metrics the mean absolute different values (center plots) were less than the within-region standard deviation of the same metric metrics (right plots). The supplemental material provides a detailed comparison of reproducibility of each metric across 35 bi-lateral gyral labels. Figure 5 illustrates representative cortical labels, sub-cortical structure, and white matter structure for a single subject.

Cortical Connectivity and Sub-Cortical Segmentation Reproducibility

Both cortical-connectivity and sub-cortical segmentations relay on multi-modal characterization of sub-cortical tissues. Section "Brain Segmentation" covers anatomical parcellation into white matter and gray matter structures; white matter characterization is discussed in Section White Matter Tract Labeling. Figure 6 examines reproducibility of cortical connectivity maps estimated by combining cortical labels and diffusion-inferred white matter tracts. Reproducibility of volumetric brain segmentations was assessed based on average Dice coefficient of rigidly registered scan-rescan data. Reproducibility of T2 lesion volumes was approximately

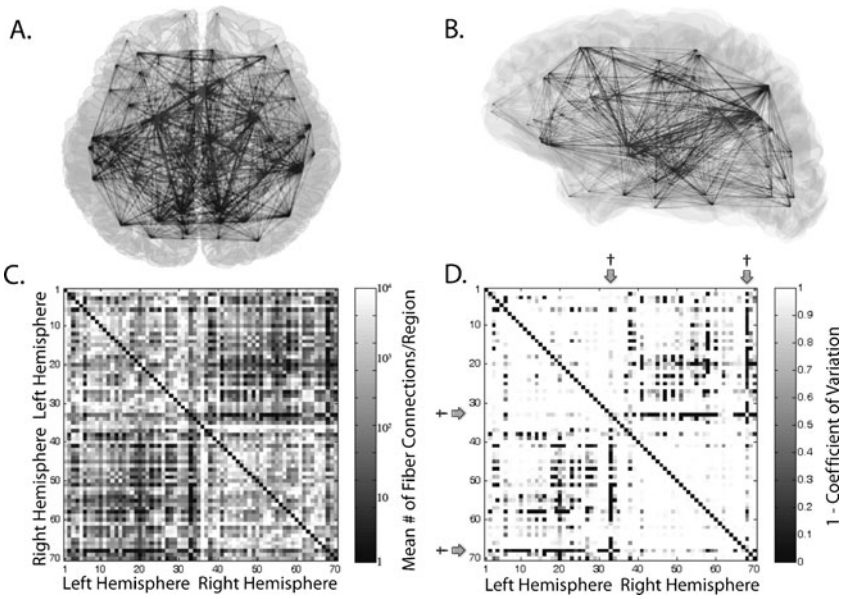

Fig. 6 Tractography mapping of cortical connectivity. The 35 bi-lateral cortical labels (see Appendix A) that were automatically identified were used as target regions for deterministic tractography. Strength of connections in terms of number of fibers per region pair are graphically illustrated in (**a**) and (**b**). **c** presents the average pair-wise regional connectivity between the 21 subjects, while **d** presents the reproducibility of connectivity strength

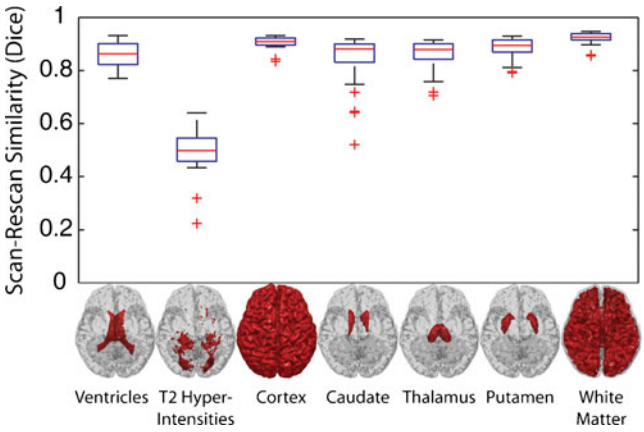

Fig. 7 Scan-rescan reproducibility of volumetric segmentation resulting from lesion TOADS. Inlays show representative brain structure volumes for each region of interest

0.5 Dice and reflective of the high surface/volume ratio of the identified lesions (so that small surface shifts resulted in proportionally large volumetric changes) and the task difficulty of distinguishing low contrast lesion boundaries. Note that the reproducibility of the remaining structures remained high despite the fact that variability in lesion classification is necessarily reflected in label exchange with other structures. Figure 7 presents scan-rescan Dice similarity between each of the brain volumes estimated by lesion-TOADS. Note that content of this figure is similar to Table 6 of (Landman et al. 2011), but using the lesion Toads in SINAPS as opposed to the stand-alone TOADS algorithm. Finally, reproducibility of tract structures was assessed via Dice overlap and is reported in Fig. 8. Smaller and more variable structures have a lower Dice (0.6–0.7), and more regular and larger ones yield superior results in the range (0.7–0.8). Dice overlap in the lesion areas are particularly low as this a healthy population. One possible explanation for the lower Dice overlap measures is that these white matter tracts are of similar size or smaller than sub-cortical structures and more elongated. Alternatively, accuracy may simply be lower given increased task difficulty (Fig. 7).

Discussion

SINAPS presents a consistent, open-source platform which is well-positioned to examine the relationship between damage to specific white matter tracts (as defined by the presence of lesions or other diffusion metrics) and changes in subcortical or cortical geometry defined within specific structural networks. SINAPS uses multiple MR images to segment both normal brain tissue and white matter lesion while preserving topology. The ability to segment white matter tracts while being robust to crossing and kissing fibers allows definition of meaningful regions of interest within the white matter, as well as the ability to automatically label tractography. This manuscript reviews the individual software modules that are used to construct the pipeline and characterize the reproducibility of the observed measures.

Although the processing and analysis techniques described here have been developed for multi-modality studies, the algorithms are modular, allowing a complete analysis to be undertaken when a subset of the potential modalities are available. Each of the processing steps in the SINAPS pipeline may also be used in isolation or replaced with a different algorithm with the same inputs and outputs. The JIST structure permits open collaboration using a shared-source archive (JIST), contributed modules from third parties are automatically included for distribution. In conclusion, SINAPS is one viable option of many that can work with rich imaging data sets, offering diverse capabilities under a single user interface.

The synergies between SINAPS and JIST provide strong opportunities for community involvement in development of related and derivative image processing pipelines. As with other permissively licensed, open-source software

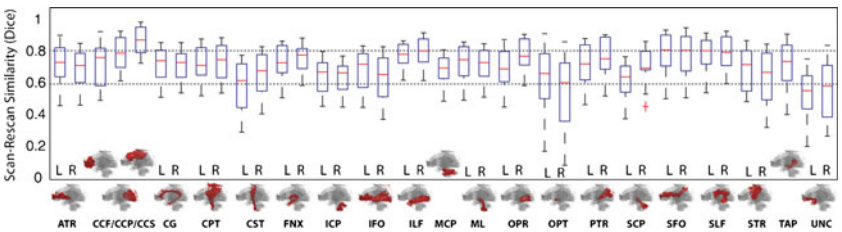

Fig. 8 Scan-rescan reproducibility of white matter tract segmentation resulting from DOTS by white matter tract structure. Inlays illustrate representative tract locations in red: *ATR* anterior thalamic radiation, *CCF/CCP/CCS* corpus callosum frontal/posterior/superior, *CG* cingulum, *CPT* cortico-pontine tract, *CST* cortico-spinal tract, *FNX* fornix, *ICP* inferior cerebellar peduncle, *IFO* inferior fronto-occipital tract, *ILF* inferior longitudinal fascicle, *MCP* middle cerebellar peduncle, *ML* medial lemniscus, *OPR* optic radiation, *OPT* optic tract, *PTR* posterior thalamic radiation, *SCP* superior cerebellar peduncle, *SFO* superior fronto-occipital fascicle, *SLF* superior longitudinal fascicle, *STR* superior thalamic radiation, *TAP* tapetum, *UNC* uncinate fascicle). Symmetric tracts are illustrated with one glyph, but reproducibility is show separately for left (L) and right (R) divisions

tools, users may modify, optimize and combine tools for their particular research needs for both internal use and redistribution. In contrast to many other platforms, pipelines, modules, modifications, optimizations to JIST are permitted (and encouraged) to be distributed with the primary analysis platform. The code base is accessible to any NITRC user and plugins contributed to this library are automatically deployed with the default release.

Information Sharing Statement

Source code and binary programs developed in this paper are available via Neuroimaging Informatics Tools and Resources Clearinghouse (NITRC: http://www.nitrc.org/projects/jist). The 'DOTS' module is available separately in open source from the DOTS WM tract segmentation project at http://www.nitrc.org/projects/dots/. These tools build upon the Medical Image Processing Analysis and Visualization (MIPAV: http://mipav.cit.nih.gov/) platform. All data are available via the Multi-Modal MRI Reproducibility Resource on NITRC (http://www.nitrc.org/projects/multimodal). The modules described herein capture the essential functionality. The details of software use and interconnections are detailed on the NITRC wiki at: http://www.nitrc.org/plugins/mwiki/index.php/jist:MultiCRUISE.

Acknowledgments The authors are appreciative of the careful feedback from the anonymous reviewers and editor (Dr. David Kennedy). This research was supported by NIH/NIA N01-AG-4-0012, NINDS 5R01NS070906, 1R03EB012461, 1R01NS056307, NIH/NIDAK25DA025356 (Bazin), and NIH/NINDSR01NS054255 (Pham).

Grant Support J. L. Prince/B. A. Landman (subcontract): NIH/NIA N01-AG-4-0012, J. Prince: 1R01NS056307, B. Landman 1R03EB012461.

Appendix A

The regions indicated in Fig. 6 are as defined by (Desikan et al. 2006) and indexed as follows. 1 : L-Subcortical Region, 2 : L-Banks of Superior Temporal Sulcus, 3 : L-Caudal Anterior Cingulate, 4 : L-Caudal Middle Frontal, 5 : L-Corpus Callosum, 6 : L-Cuneus, 7 : L-Entorhinal 8 : L-Fusiform, 9 : L-Inferior Parietal, 10 : L-Inferior Temporal, 11 : L-Isthmus, 12 : L-Lateral Occipital, 13 : L-Lateral Orbitofrontal, 14 : L-Lingual, 15 : L-Medial Orbitofrontal, 16 : L-Middle Temporal, 17 : L-Parahippocampal, 18 : L-Paracentral, 19 : L-Pars Opercularis, 20 : L-Pars Orbitalis, 21 : L-Pars Triangularis, 22 : L-Pericalcarine, 23 : L-Postcentral, 24 : L-Posterior Cingulate, 25 : L-Precentral, 26 : L-Precuneus, 27 : L-Rostral Anterior Cingulate, 28 : L-Rostral Middle Frontal, 29 : L-Superior Frontal, 30 : L-Superior Parietal, 31 : L-Superior Temporal, 32 : L-Supramarginal, 33 : L-Frontal Pole, 34 : L-Temporal Pole, 35 : L-Transverse Temporal, 36 : R-Subcortical Region, 37 : R-Banks of the Superior Temporal Sulcus, 38 : R-Caudal Anterior Cingulate, 39 : R-Caudal Middle Frontal, 40 : R-Corpus Callosum, 41 : R-Cuneus, 42 : R-Entorhinal, 43 : R-Fusiform, 44 : R-Inferior Parietal, 45 : R-Inferior Temporal, 46 : R-Isthmus, 47 : R-Lateral Occipital, 48 : R-Lateral Orbitofrontal, 49 : R-Lingual, 50 : R-Medial Orbitofrontal, 51 : R-Middle Temporal, 52 : R-Parahippocampal, 53 : R-Paracentral, 54 : R-Pars Opercularis, 55 : R-Pars Orbitalis, 56 : R-Pars Triangularis, 57 : R-Pericalcarine, 58 : R-Postcentral, 59 : R-Posterior Cingulate, 60 : R-Precentral, 61 : R-Precuneus, 62 : R-Rostral Anterior Cingulate, 63 : R-Rostral Middle Frontal,64 : R-Superior Frontal, 65 : R-Superior Parietal, 66 : R-Superior Temporal, 67 : R-Supramarginal, 68 : R-Frontal Pole, 69 : R-Temporal Pole, 70 : R-Transverse Temporal

References

Andersson, J. L. R., Skare, S., & Ashburner, J. (2003). How to correct susceptibility distortions in spin-echo echo-planar images: application to diffusion tensor imaging. *NeuroImage, 20*, 870–888.

Ashburner, J., & Friston, K. J. (2000). Voxel-based morphometry–the methods. *NeuroImage, 11*(6 Pt 1), 805–821.

Awate, S.P. and Gee, J.C. (2007). *A fuzzy, nonparametric segmentation framework for DTI and MRI analysis*, In *Proceedings of the International Conference on Information Processing in Medical Imaging 2007 (IPMI'07)*. Kerkrade.

Bazin, P. L., & Pham, D. L. (2007a). Topology-preserving tissue classification of magnetic resonance brain images. *IEEE Transactions on Medical Imaging, 26*(4), 487–496.

Bazin, P. L., & Pham, D. L. (2007b). Topology correction of segmented medical images using a fast marching algorithm. *Computer Methods and Programs in Biomedicine, 88*(2), 182–190.

Bazin, P.-L., & Pham, D. L. (2008). Homeomorphic brain image segmentation with topological and statistical atlases. *Medical Image Analysis, 12*, 616–625.

Bazin, P. L., et al. (2011). Direct segmentation of the major white matter tracts in diffusion tensor images. *NeuroImage, 58*(2), 458–468.

Beg, F., Miller, M., Trouve, A., & Younes. (2005). Computing large deformation metric mappings via geodesic flows of diffeomorphisms. *International Journal of Computer Vision, 23*(2), 108–118.

Bogovic, J., et al. (2010). *Statistical fusion of surface labels provided by multiple raters, over-complete, and ancillary data*. In *SPIE Medical Imaging Conference*. San Diego, CA.

Brain Innovation B.V. (2007) *BrainVoyager*. Available from: http://www.brainvoyager.com/.

Carass, A., et al. (2011). Simple paradigm for extra-cerebral tissue removal: algorithm and analysis. *NeuroImage, 56*(4), 1982–1992.

Chen, M., et al. (2010). *Multi-channel enhancement of the adaptive bases algorithm*, In *Organization for Human Brain Mapping*. Barcelona, Spain.

Cointepas, Y., et al. (2001). BrainVISA: Software platform for visualization and analysis of multi-modality brain data. *NeuroImage, 13*(6), S98.

Covington, K. et al. (2010). *Interfaces and integration of medical image analysis frameworks: Challenges and Opportunities*. In *Biomedical Science and Engineering Conference*. Oak Ridge, TN.

Covington, K., Welch, E.B. and Landman, B.A. (2011). *Integrating medical imaging analyses through a high-throughput bundled resource imaging system*. In *SPIE Medical Imaging Conference*. Lake Buena Vista, Florida.

Dale, A. M., Fischl, B., & Sereno, M. I. (1999). *Cortical surface-based analysis.* I. Segmentation and surface reconstruction. *Neuroimage, 9*(2), 179–194.

Desikan, R. S., et al. (2006). An automated labeling system for subdividing the human cerebral cortex on MRI scans into gyral based regions of interest. *NeuroImage, 31*(3), 968–980.

Eckstein, I., et al. (2009). Active fibers: Matching deformable tract templates to diffusion tensor images. *Neuroimage, 47*(Supplement 2), T82–T89.

El Kouby, V., et al. (2005). *MR Diffusion-based inference of a fiber bundle model from a population of subjects*, In *Proceedings of the 8th International Conference on Medical Image Computing and Computer-Assisted Intervention (MICCAI'05)*. Palm Springs.

Fischl, B., Sereno, M. I., & Dale, A. M. (1999). Cortical surface-based analysis. II: Inflation, flattening, and a surface-based coordinate system. *NeuroImage, 9*(2), 195–207.

Friston, K., (2006) *Statistical parametric mapping: The analysis of functional brain images* (p. 656). Academic Press.

Han, X., et al. (2001). *Cortical surface reconstruction using a topology preserving geometric deformable model*. In *5th IEEE Workshop on Mathematical Methods in Biomedical Image Analysis (MMBIA2001)*. Kauai, Hawaii.

Han, X., Xu, C., & Prince, J. L. (2003). A topology preserving level set method for geometric deformable models. *IEEE Transactions on Pattern Analysis and Machine Intelligence, 25*, 755–768.

Han, X., et al. (2004). CRUISE: cortical reconstruction using implicit surface evolution. *NeuroImage, 23*(3), 997–1012.

Jezzard, P., & Balaban, R. S. (1995). Correction for geometric distortion in echo planar images from B0 field variations. *Magnetic Resonance in Medicine, 34*, 65–73.

Jezzard, P., Barnett, A. S., & Pierpaoli, C. (1998). Characterization and correction for Eddy current artifacts in echo planar diffusion imaging. *Magnetic Resonance in Medicine, 39*, 801–812.

Jones, D. K. (2008). Studying connections in the living human brain with diffusion MRI. *Cortex, 44*(8), 936–952.

Koenderink, J. J., & van Doorn, A. J. (1992). Surface shape and curvature scales. *Image and Vision Computing, 10*(8), 557–565.

Landman, B. A., et al. (2007). Effects of diffusion weighting schemes on the reproducibility of DTI-derived fractional anisotropy, mean diffusivity, and principal eigenvector measurements at 1.5T. *Neuroimage, 36*(4), 1123–1138.

Landman, B., et al. (2011). Multi-parametric neuroimaging reproducibility: A 3T resource study. *NeuroImage, 4*(14), 2854–2866.

Lawes, I. N. C., et al. (2008). Atlas-based segmentation of white matter tracts of the human brain using diffusion tensor tractography and comparison with classical dissection. *NeuroImage, 39*, 62–79.

Lenglet, C., Rousson, M., & Deriche, R. (2006). DTI segmentation by statistical surface evolution. *IEEE Transactions on Medical Imaging, 25*(6), 685–700.

Lucas, B. C., et al. (2010). The Java Image Science Toolkit (JIST) for rapid prototyping and publishing of neuroimaging software. *Neuroinformatics, 8*(1), 5–17.

MacDonald, D., et al. (2000). Automated 3-D extraction of inner and outer surfaces of cerebral cortex from MRI. *NeuroImage, 12*(3), 340–356.

Maddah, M., et al. (2007). *Probabilistic clustering and quantitative analysis of white matter fiber tracts*, In *Proceedings of the International Conference on Information Processing in Medical Imaging 2007 (IPMI'07)*. Kerkrade.

Maddah, M. et al. (2008). *A mathematical framework for incorporating anatomical knowledge in DT-MRI analysis*, In *Biomedical Imaging: From Nano to Macro, 2008. ISBI 2008. 5th IEEE International Symposium on Biomedical Imaging* (p. 105–108). Paris, France.

Maes, F., et al. (1997). Multimodality image registration by maximization of mutual information. *IEEE Transactions on Medical Imaging, 16*(2), 187–198.

Mangin, J.-F., et al. (1995). From 3D magnetic resonance images to structural representations of the cortex topography using topology preserving deformations. *Journal of Mathematical Imaging and Vision, 5*, 297–318.

Marcus, D., et al. (2007). Open Access Series of Imaging Studies (OASIS): cross-sectional MRI data in young, middle aged, nondemented, and demented older adults. *Journal of Cognitive Neuroscience, 19*(9), 1498–1507.

Mori, S., et al. (1999). Three-dimensional tracking of axonal projections in the brain by magnetic resonance imaging. *Annals of Neurology, 45*(2), 265–269.

Mori, S. et al. (2005). *MRI Atlas of human white matter*. Elsevier.

Mueller, S. G., et al. (2005). Ways toward an early diagnosis in Alzheimer's disease: the Alzheimer's Disease Neuroimaging Initiative (ADNI). *Alzheimer's & Dementia, 1*(1), 55–66.

Pechura, C.M. and Martin, J.B. (1991). *Mapping the brain and its functions. integrating enabling technologies into neuroscience research*. National Academy Press.

Pham, D. L., & Prince, J. L. (1999). Adaptive fuzzy segmentation of magnetic resonance images. *IEEE Transactions on Medical Imaging, 18*(9), 737–752.

Pieper, S., et al. (2006). *The NA-MIC Kit: ITK, VTK, pipelines, grids and 3D slicer as an open platform for the medical image computing community*. in *3rd IEEE International Symposium on Biomedical Imaging: Nano to Macro*.

Riviere, D., et al. (2002). Automatic recognition of cortical sulci of the human brain using a congregation of neural networks. *Medical Image Analysis, 6*(2), 77–92.

Rohde, G. K., Aldroubi, A., & Dawant, B. M. (2003). The adaptive bases algorithm for intensity-based nonrigid image registration. *IEEE Transactions on Medical Imaging, 22*(11), 1470–1479.

Rohde, G. K., et al. (2004). Comprehensive approach for correction of motion and distortion in diffusion-weighted MRI. *Magnetic Resonance in Medicine, 51*, 103–114.

Sethian, J. A. (1999). *Level Set Methods and Fast Marching Methods. Vol. second ed*. Cambridge: Cambridge Univ. Press.

Shattuck, D. W., & Leahy, R. M. (2000). *BrainSuite: An automated corticalsurface identification tool. in Lecture Notes in Computer Science. Medical Image Computing and Computer-Assisted Intervention MICCAI*. Berlin: Springer.

Shiee, N., et al. (2008). *Automated reconstruction of the cerebral cortex in multiple*. In *Sixth IEEE International Symposium on Biomedical Imaging (ISBI)*.

Shiee, N., et al. (2010). A Topology-preserving approach to the segmentation of brain images with multiple sclerosis lesions. *NeuroImage*, 1524–1535.

Smith, S. M., et al. (2004). Advances in functional and structural MR image analysis and implementation as FSL. *NeuroImage, 23* (Suppl 1), S208–S219.

Sporns, O., et al. (2004). Organization, development and function of complex brain networks. *Trends in Cognitive Science, 8*(9), 418–425.

Thambisetty, M., et al. (2010). Longitudinal changes in cortical thickness associated with normal aging. *NeuroImage, 52*(4), 1215–1223.

Thompson, P. M., & Toga, A. W. (2002). A framework for computational anatomy. *Computing and Visualization in Science, 5*, 1–12.

Tosun, D., Rettmann, M.E. and Prince, J.L. (2003). *Mapping techniques for aligning sulci across multiple brains*, in *Proceedings of The Sixth Annual International Conference on Medical Image*

Computing and Computer-Assisted Interventions(MICCAI). Montréal.

Tosun, D., Rettmann, M., & Prince, J. (2004). Mapping techniques for aligning sulci across multiple brains. *Medical Image Analysis, 8* (3), 295–309.

Van Essen, D. C., et al. (2001). An integrated software suite for surface-based analyses of cerebral cortex. *Journal of the American Medical Informatics Association, 8*(5), 443–459.

van Leemput, K., et al. (1999). Automated model-based tissue classification of MR images of the brain. *IEEE Transactions on Medical Imaging, 18*(10), 897–908.

Viola, P. and Wells, W.M. (1995). *Alignment by maximization of mutual information*. In *Proc. 5th Int. Conf. on Computer Vision*.

Wakana, S., et al. (2007). Reproducibility of quantitative tractography methods applied to cerebral white matter. *NeuroImage, 36*, 630–644.

Warfield, S. K., Zou, K. H., & Wells, W. M. (2004). Simultaneous truth and performance level estimation (STAPLE): an algorithm for the validation of image segmentation. *IEEE Transactions on Medical Imaging, 23*(7), 903–921.

Xu, C., et al. (1999). Reconstruction of the human cerebral cortex from magnetic resonance images. *IEEE Transactions on Medical Imaging, 18*(6), 467–480.

Zeng, X., et al. (1999). Segmentation and measurement of the cortex from 3-D MR images using coupled-surfaces propagation. *IEEE Transactions on Medical Imaging, 18*(10), 927–937.